Regular Article

PHYSICAL CHEMISTRY RESEARCH
Published by the
Iranian Chemical Society
www.physchemres.org
info@physchemres.org

Phys. Chem. Res., Vol. 6, No. 2, 237-250, June 2018
DOI: 10.22036/pcr.2017.98758.1417

pH Effect on the Size of Graphene Quantum dot Synthesized by Using Pulse Laser Irradiation

M. Aghelifar[a] and S. Kimiagar[b,*]

[a]*Department of Physics, Central Tehran Branch, Islamic Azad University, Iran*
[b]*Nano Research Lab (NRL), Department of Physics, Central Tehran Branch, Islamic Azad University, Iran*

(Received 24 September 2017, Accepted 26 November 2017)

In this study graphene oxide (GO) is synthesized by using Hummer's method. Low dimension graphene quantum dot nanoparticles (GQDs) are synthesized using pulse laser irradiation. Fourier transform-infrared spectroscopy (FTIR), ultraviolet-visible (UV-Vis) spectroscopy and photoluminescence (PL) analysis are applied to study the GQDs characteristic. Scanning electron microscopy illustrates the morphologies of GQDs and RGQDs. The results show that the solution's pH has an effect on the size and bandgap of GQD. We introduce a suitable method to construct GQDs with great bandgap control, indicating a bright horizon for investigating graphene's potential applications in transparent electronics, transistors, sensors, and energy harvesters. The successful attainment is size control by changing pH of solution and low cost synthesis process.

Keyword: Bandgap, Graphene, Pulse laser, Quantum dot

INTRODUCTION

Graphene has been widely used as transparent conductive electrodes in solar cells, light-emitting diodes (LEDs) and touch panels [1]. A new graphene type, GQD (single-layer graphene with finite size) has appeared in theoretical studies and it has been given high interest owing to its excellent chemical and physical properties [2,3]. GQDs have unique electron transportation properties, low cytotoxicity, and excellent biocompatibility. In addition, GQDs contain an exceptional phenomenon associated with quantum confinement and edge effects [4]. These characteristics result in broad applications in various fields, such as photovoltaics [5,6]. In this line, GQDs have been identified as a cost-competitive, environmentally friendly, and stable photoactive material in various applications.

Considering the low-dimension of GQDs, they exhibit effective photocarrier generation and separation at metal oxide interface compared to graphene layers. This might cause a reduction in the charge recombination rate [7]. While the electronic and optical properties of GQDs have been rarely investigated, quantum-confined systems have been studies by some research groups [8,9]. Simultaneously, in opposition to the zero-bandgap of graphene, GQDs possess a tunable bandgap due to the quantum confinement and edge effects [10]. Two methods have been reported to control the GQDs bandgaps. In one case, the GQDs were rapidly purified using cross-flow ultrafiltration to separate them by size *via* variation of the membrane pore size [11,12]. The emission wavelengths of the purified GQDs depend on their sizes, in accord with the quantum confinement effect [4] on their functionalities and defects. In the second approach, instead of using ultrafiltration, they engineer the bandgaps of the GQDs. In ultrafiltration, the reaction temperature of the oxidation process is controlled. Consequently, size of GQDs depend on the temperature which has fluorescence in the visible range. The higher the temperature, the smaller the GQDs, emphasizing the facility with which the domain sizes could be controllable through

*Corresponding author. E-mail: kimia@khayam.ut.ac.ir

oxidative cutting [13]. Bandgap could be reached by changing the etching duration, and the oxygen component ratio in the GQDs could be also controlled by changing the etching duration to achieve the highest intensity of the bandgap [14]. The tunable bandgap of GQDs is related to both the size effect and functionality effect [15].

One of the most important properties used to classify the optical response of a quantum dot system is whether it has a direct or indirect bandgap. In dots with direct gaps, the electron and hole wave functions are both confined within the dot and are both derived from the Γ states of Brillouin zone center. Dots with indirect bandgaps can be indirect in real space. In this case, the electrons and holes are localized in different regions of the nanostructure, where the states are from different k points in the Brillouin zone [16]. On moving from a bulk system to a dot system, the level ordering can be completely changed by the effects of quantum confinement and strain. Quantum confinement drives electron levels up in energy and hole levels down in energy and strain can drive levels either up or down in energy depending on the sign of the deformation potential. If the lowest electron level in the barrier is below that of the dot, then electrons may localize in the barrier, generating a system that is indirect in real space. Similarly, if the highest hole level in the barrier is above that of the dot, then holes may localize in the barrier, again creating a system that is indirect in real space [16]. In this paper, we have synthesized GQDs with controlled bandgaps using a variety of pH under laser irradiation. The samples were analyzed by Fourier transform infrared spectroscopy, UV-Vis, scanning electron microscopy and photoluminescence.

EXPERIMENTAL DETAILS

All materials for the experiment were purchased from Merck Company. Go was synthesized by using Hummer's method. The detail can be found in our previous report [17]. GO powder was dissolved in DI water with concentration of 0.2 wt%. Then, ammonia solution and H_2O_2 were added to the GO suspension to tune pH (Shanghai Precision Scientific Instrument Co.). Then stirred 15 min to produce homogenous solution. The resulted solution was transferred into a 100 ml Teflon-lined stainless-steel autoclave and heated to 150 ℃ for 5 h. After being cooled down to room temperature, the obtained solution filtered by PTFE membrane (millipore, pore size: 100 nm). The process was repeated four times with various pH = 5, 9, 11, 13 and the samples named GQD-5, GQD-9, GQD-11, GQD-13, respectively.

Then, 8 ml GQDs solution with various PH were exposed to ND:YAG pulsed laser system (Quantel, Briliant b class4 with 532 nm wavelength, 5 ns pulse duration, 10 Hz repetition rate, 0.3 W power, and 40 mJ maximum pulse energy in 7 mm beam diameter)for 5 min. The fabricated samples were tagged RGQD-5, RGQD-9, RGQD-11 and RGQD-13. Ultimately eight different GQDs and RGQDs were synthesized, which are shown in Table 1.

Morphologies and structures of GQDs were investigated by Fourier transform infrared (FTIR) spectroscopy (jasco FTIR-410) and scanning electron microscopy (SEM, VEGA/TESCAN-XMU). Dynamic light scattering (DLS, Malvern Instruments MAL1008078) was applied to study the size of GQD. PL and UV-Vis spectra were measured by a fluorescence spectrometer (PL, perkinelmer LS 45) and UV-Vis spectrophotometer (Lambda 750).

RESULTS AND DISCUSSION

In order to characterize the functionalization of GO and GQDs in the frequency range for stretching and bending modes, FTIR spectra were used (Fig. 1). GO and GQDs both displayed the aromatic of C=C (1572 cm^{-1}), stretching vibrations of C=O (1732 cm^{-1}), and C-O-C (2326 cm^{-1}) [18, 19]. Functionalized groups were on the edges O-H (3396 cm^{-1}) and (1418 cm^{-1}), C-H (2789 cm^{-1}) [20]. The small peak was observed at 2900 cm^{-1}, such features are not easily detected as the size of the GQDs grows. This is associated with declining abundance of edge C-H stretching as the GQDs grow in size [13]. However, the O-H stretching vibration of GO was deteriorated compared to that of GQDs. Vibrations of C-O-H at 1230 cm^{-1} in the GQDs spectrum [18], also appeared. The structure of the GO is split less at the surface in comparison with the border. In addition to active peaks the functionalization group C-O-OH at 1410 cm^{-1} can be observed for the GQDs.

Figures 2 and 3 show the UV-Vis absorption spectra of GQDs and RGQDs synthesized at pH = 5, 9, 11 and 13. RGQD and GQD absorptions are increased both at the

Table 1. Eight Different GQDs and RGQDs Samples

Sample	GQD-5	GQD-9	GQD-11	GQD-13	RGQD-5	RGQD-9	RGQD-11	RGQD-13
Laser	Off	Off	Off	Off	On	On	On	On
pH	5	9	11	13	5	9	11	13

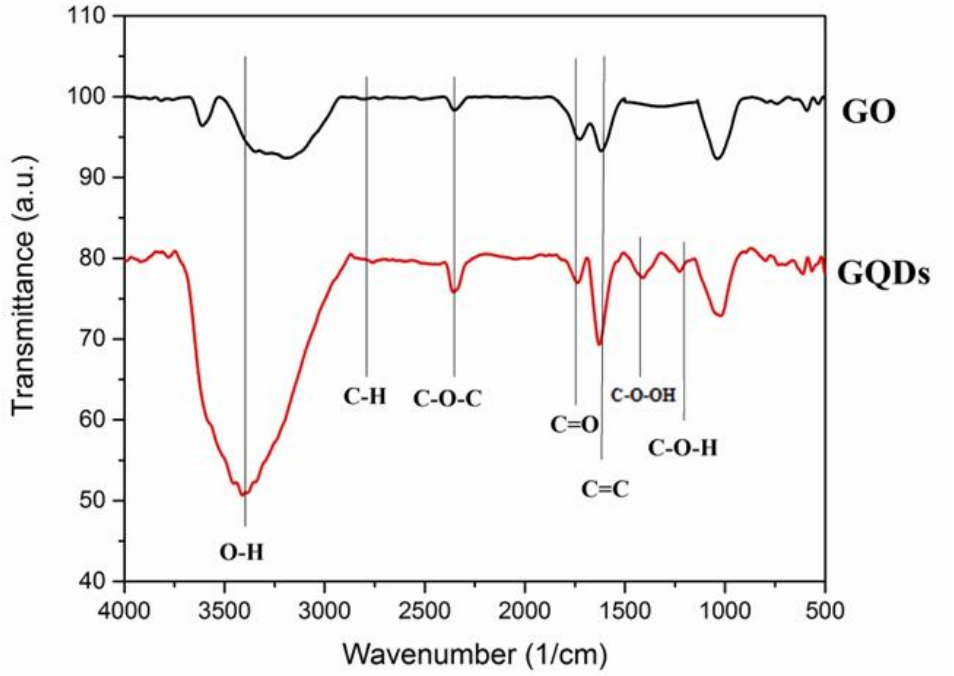

Fig. 1. FTIR spectra of GO and GQDs.

ultraviolet and visible regions of the spectrum. The high absorbance was observed at UV region which is associated with the π-π* transition of aromatic sp^2 domains in GQDs and RGQDs [2]. The visible light absorption is originated from the excitation between σ and π orbital to the lowest unoccupied molecular orbital [21]. RGQDs compared to GQDs show higher and broader absorption spectrum with a steady change up to 700 nm. This indicates the existence of band tail by defect states.

The bandgap is determined by using the relation:

$$\alpha = \frac{A(h\upsilon - E_g)^n}{h\upsilon} \quad (1)$$

where *hv* is the photon energy, *Eg* the optical bandgap, α is absorption coefficient and A is the constant related to the effective masses associated with the valence and conduction bands. The *n = 1/2* and *n = 2* are for allowed direct and indirect transitions, respectively.

There are several physical factors dominating the bandgap of GQDs in terms of being direct or indirect. The initial level ordering in the bulk material from which the dot is obtained is as follows: the size of the quantum dot, the GQDs fabrication method, growth technique, strain changes and quantum confinement affecting the type and amount of the GQDs bandgap. Different values of GQDs' bandgap have been reported in several studies. Senlin Diao et al. have reported optical bandgaps to be ~3.60 eV, ~2.93 eV,

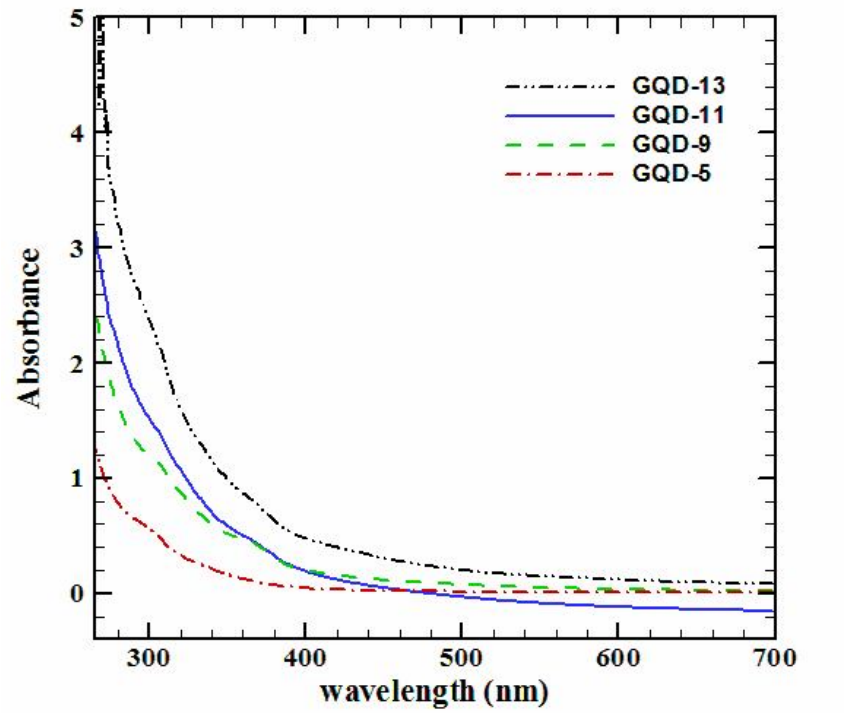

Fig. 2 Absorption spectra of the GQDs at various pHs.

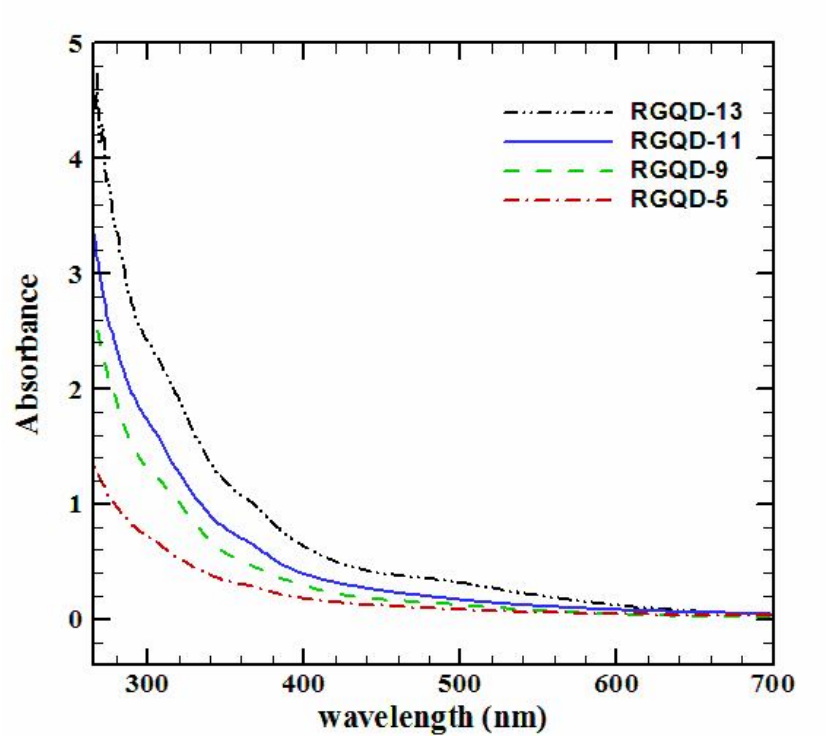

Fig. 3. Absorption spectra of the RGQDs at various pHs.

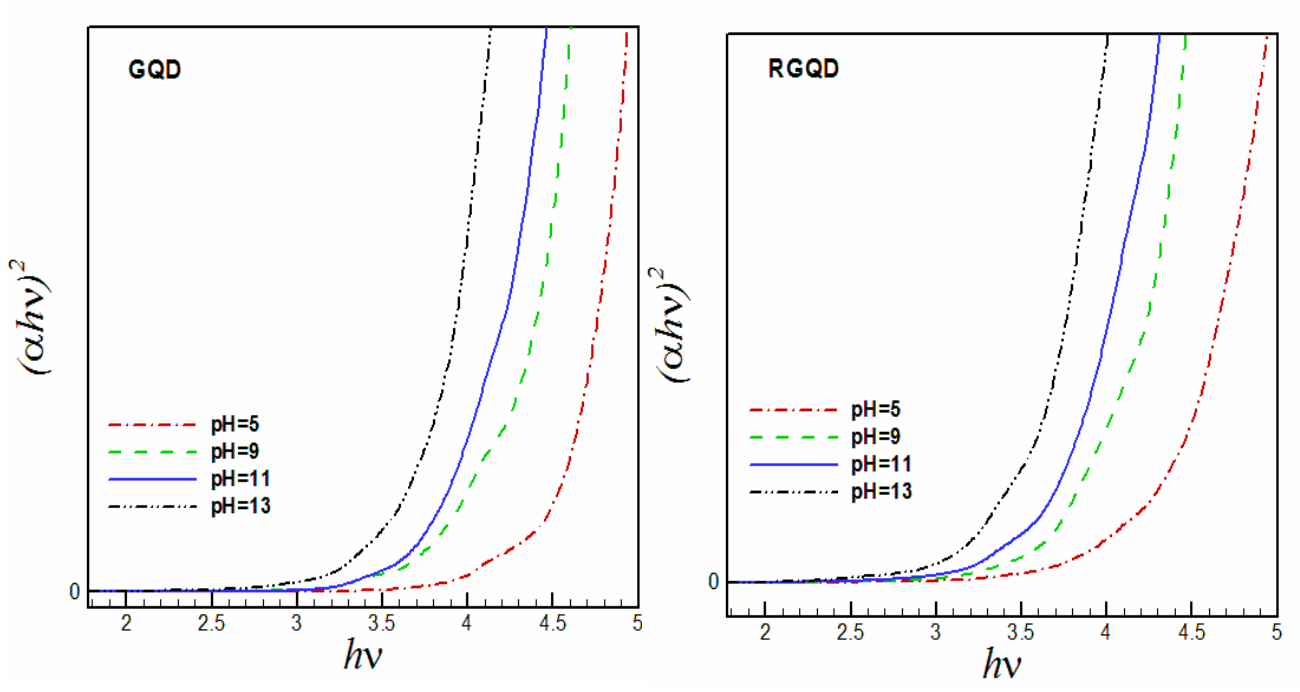

Fig. 4. Direct bandgaps of GQDs and RGQDs.

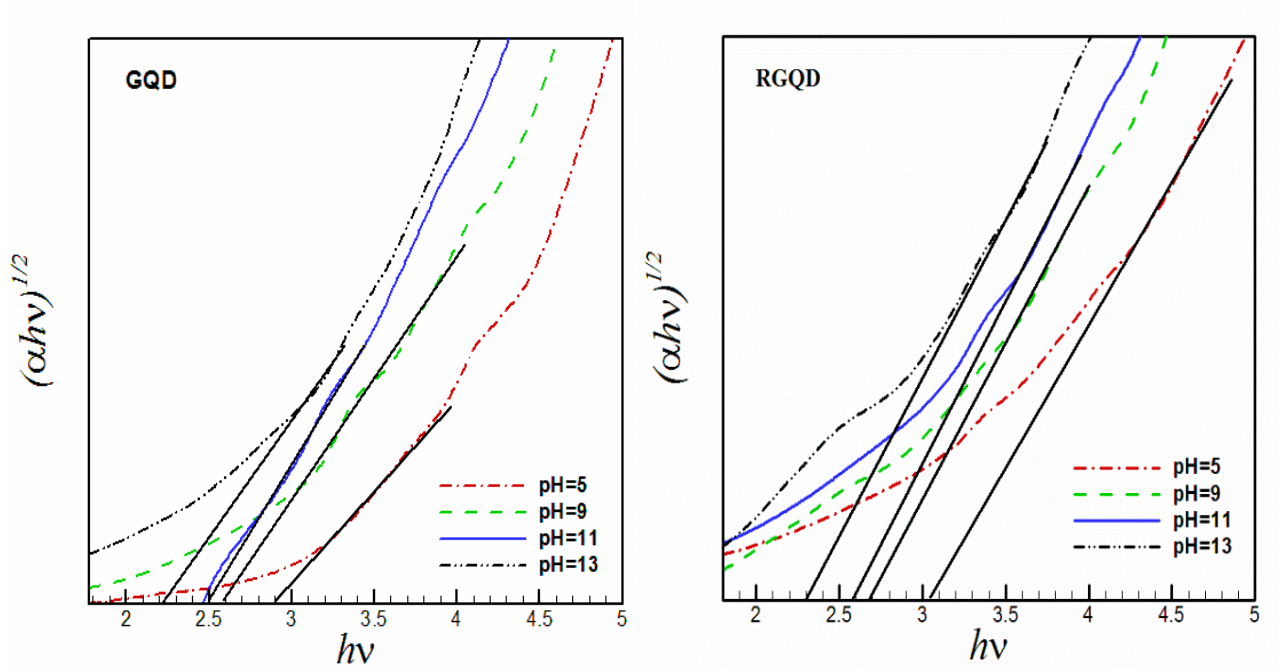

Fig. 5. Indirect bandgaps of GQDs and RGQDs.

Table 2. Calculated Bandgaps for the GQDs and RGQDs

pH	5	9	11	13
GQD bandgap (eV)	2.9	2.6	2.5	2.2
RGQD bandgap (eV)	3.1	2.7	2.6	2.3

and ~2.27 eV for various sizes [22]. To further understand the bandgaps, both direct and indirect bandgaps were calculated and the results can be seen in Figs. 4 and 5, respectively. It is obvious that direct bandgap is in the range of 3.5 up to 4.5 eV, in consistent with the results of PL and UV analyses. Accordingly, bandgap should be in the range of 2.5 up to 3.5, in consistent with indirect bandgap calculation. The calculated bandgaps are shown in Table 2.

In fact, the bandgap of GQDs is strongly influenced by the size of GQDs owing to the quantum confinement effect. Ritter *et al*. [23] and Lu *et al*. [24] demonstrated the size dependence of the GQDs' bandgap. These authors demonstrated that the bandgap of the GQDs increases as the size of the GQDs decreases. Peng *et al*. [2] have reported that the PL emission is blue shifted by decreasing the size and increasing the bandgap of GQDs.

In order to estimate the size of GQDs, DLS analysis was applied. Figures 6 and 7 show DLS of GQDs before and after laser irradiation. The results are indicated in Table 3 which is compatible with bandgap calculation (Table 2). After laser irradiation the size of RGQDs is clearly reduced. This reduction for higher pH is more than that for lower pH. Figure 8 indicates the SEM image of dried (without using vacuumed conditions) GQDs. Different sizes of GQDs with closed pores on the surface are distributed. GQDs are agglomerated while drying the droplets on glass. The average aggregate size expands when pH is enhanced from 5 to 13. The change in size-distribution as well as in shape of the aggregates of the condensate implied a powerful effect of solvent pH on the structure of aggregates. Surface characteristics affect agglomeration in dispersions, and the nanoparticle hydrodynamic size distributions could be modified by a small transformation of particle surface charge [25]. The hydrodynamic size can be altered by changing the solution pH. The charge on the surface is influenced by several mechanisms including surface ionization, ion adsorption, and lattice ion dissolution. It was found that when nanoparticles are dispersed in liquids, their hydrodynamic size is often bigger than the initial particle size. The agglomeration nature of nanoparticles under different pH of solution is apparent form SEM images (Fig. 8) [26]. After laser irradiation and reduction of GQDs the size of RGQDs are smaller than that of GQDs and less aggregation occurs (Fig. 9).

Figures 10 and 11 show the photoluminescence (PL) spectra (340 nm excitation wavelength) of the aqueous solution of GQDs and RGQDs, respectively. A broad and strong emission peak at 445 and 440 nm related to GQDs and RGQDs is seen due to quantum confinement of GQDs. This blue-shift in maximum is associate to the wider bandgap and smaller size after laser irradiation [13]. It confirms the findings of previous works describing the luminescence mechanism of GQDs [13]. The PL spectrum guarantees the visible light bandgap of GQDs and RGQDs. The visible light activity of GQDs was tested with optical absorbance spectra, which clearly reveals that the band edge falls above 300 nm (Figs. 2 and 3).

Our knowledge and understanding of the PL properties of GQDs are still insufficient; other possible mechanisms have been proposed, such as size effect, surface modification and oxidation. However, it has been challenging to clearly determine the source of pure GQDs, since many defect states including functional groups carrying oxygen still exist in GQDs and RGQDs with structural deformation. PL behavior changes from GQDs to RGQDs. Previous reports support that defect state emission (surface energy traps) and intrinsic state emission (electron-hole recombination, quantum size effect/zig-zag sites) make a contribution to fluorescence synchronously [27-31]. Zhu *et al*. have explained that initial green luminescent GQDs

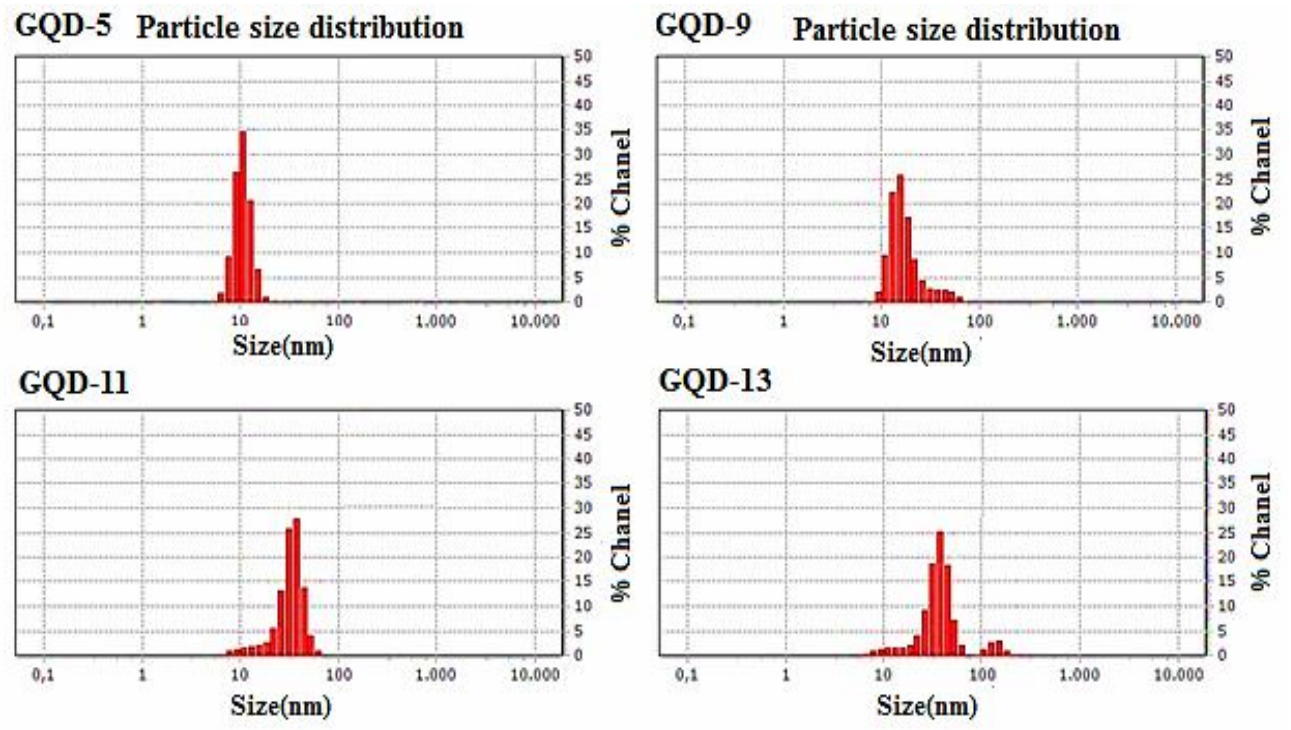

Fig. 6. Size distribution of GQDs.

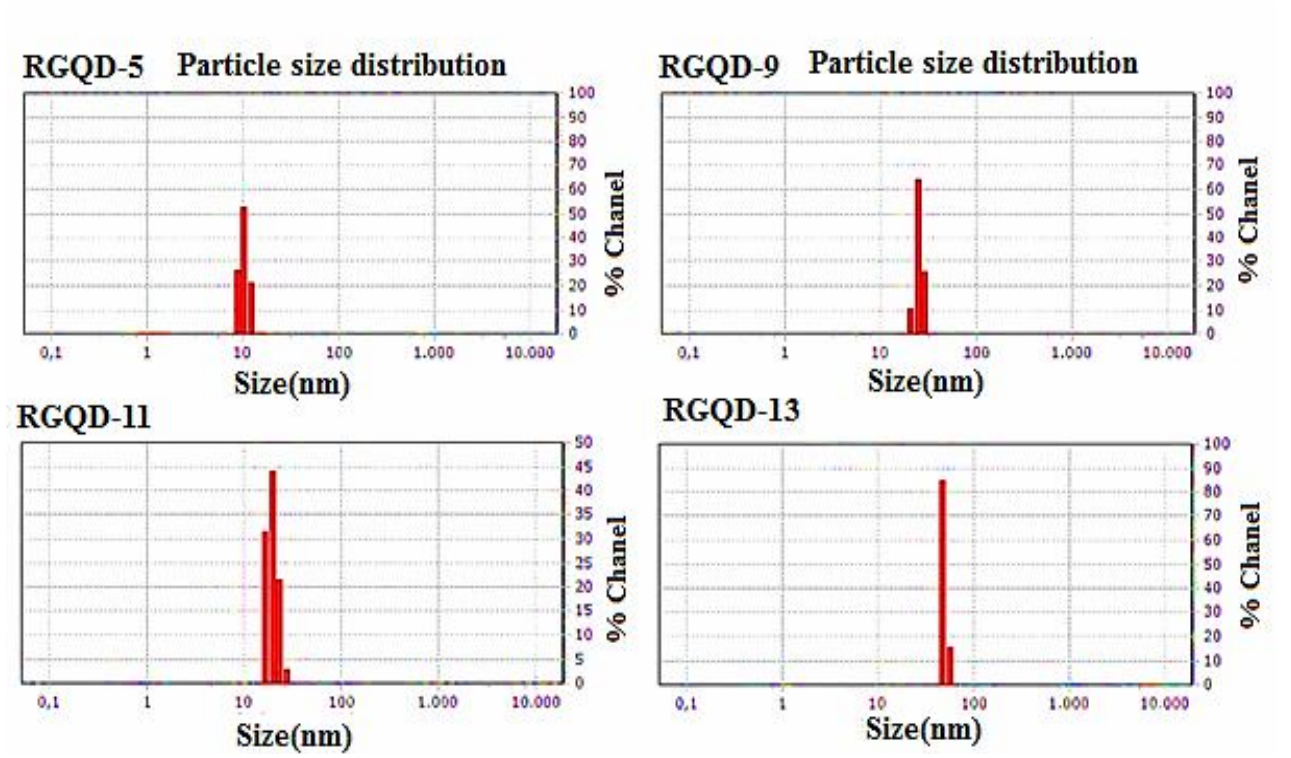

Fig. 7. Size distribution of RGQDs.

Table 3. DLS Results for GQDs and RGQDs

pH	5	9	11	13
GQD (nm)	13	38	68	92
RGQD (nm)	10	30	55	74

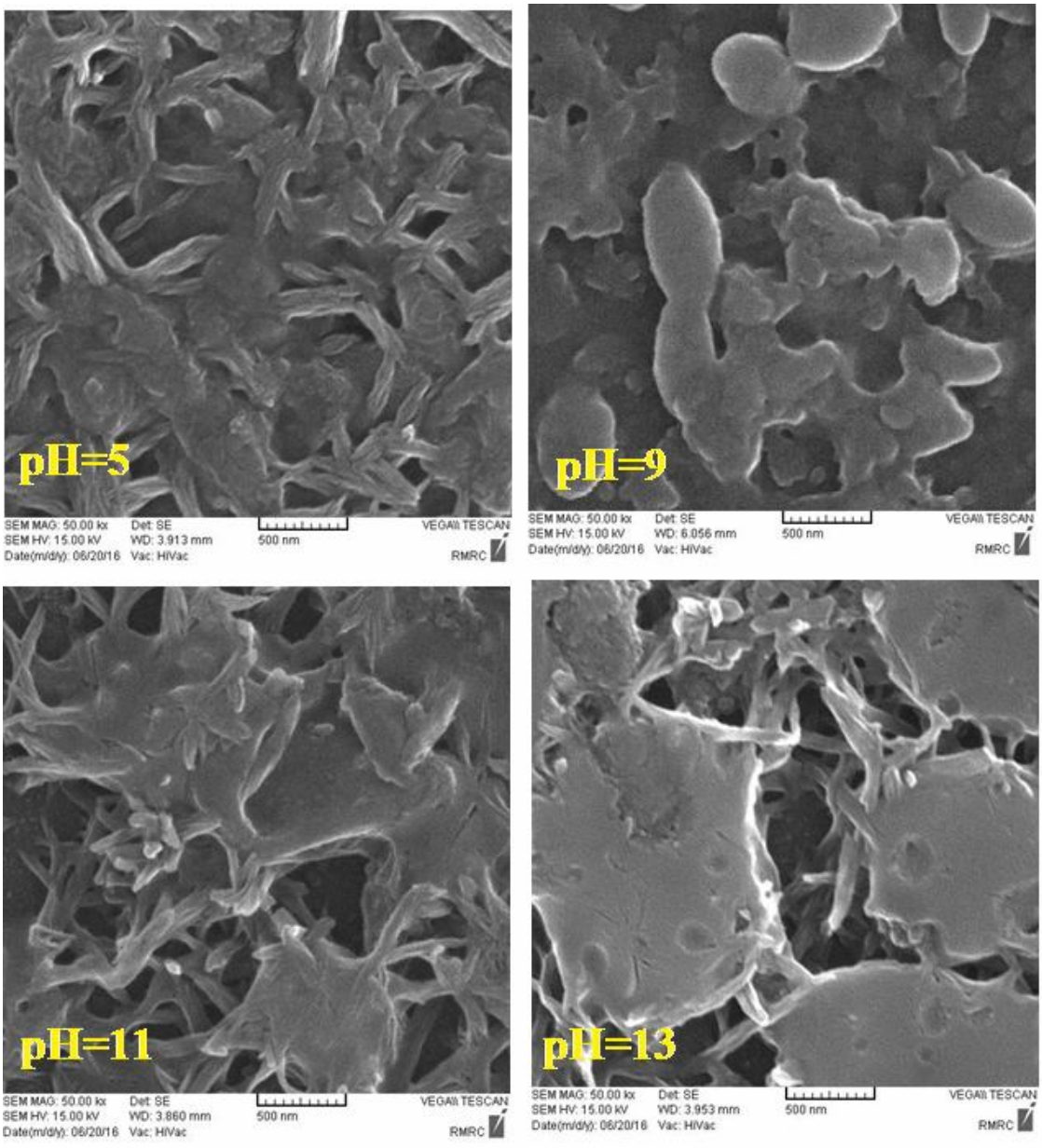

Fig. 8. SEM image of GQDs at different pHs.

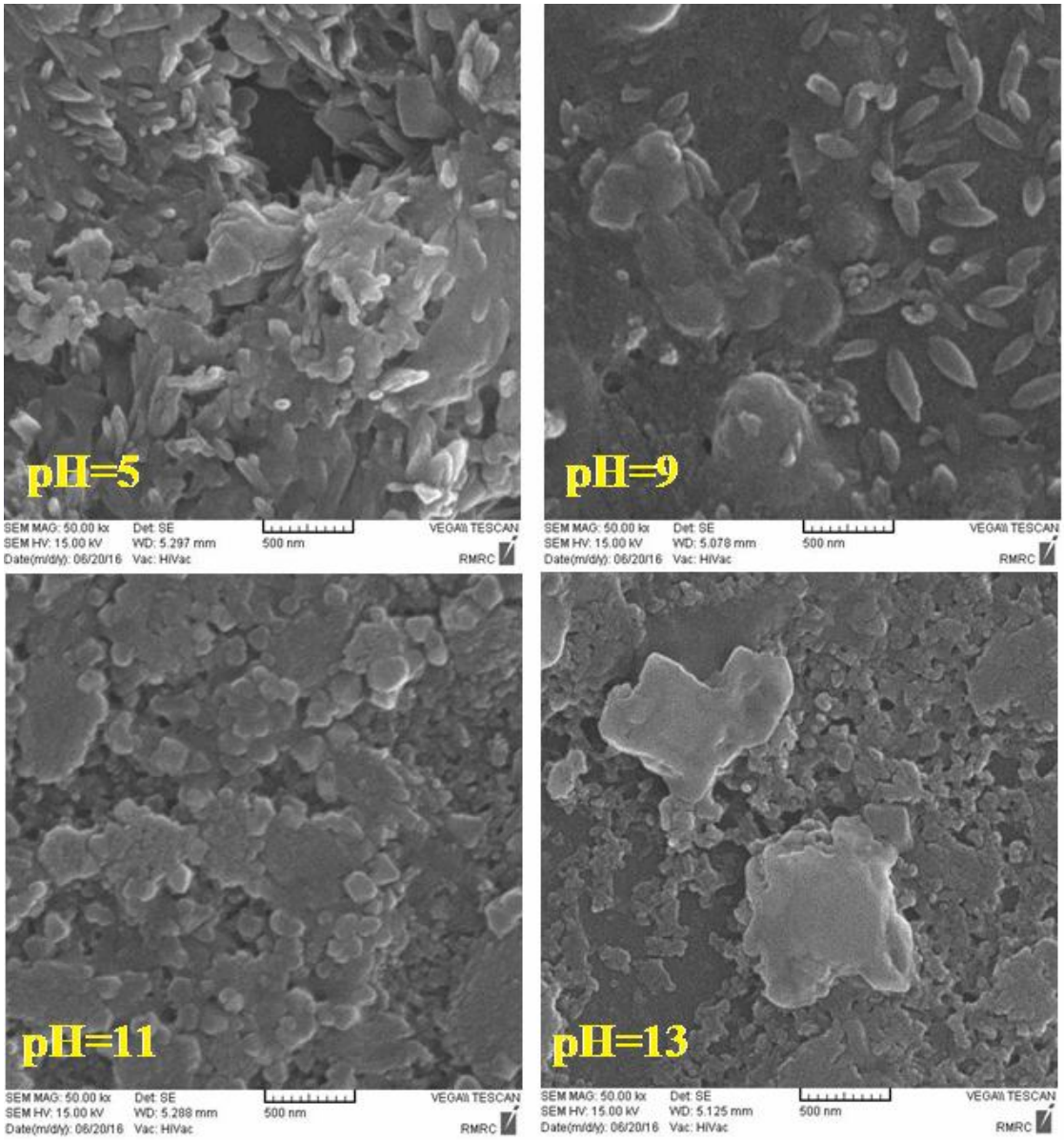

Fig. 9. SEM image of RGQDs at different pHs.

have two emission peaks, one is around 440 nm (blue emission) and the other one is at 516 nm (green emission). The blue emission is related to electron-hole recombination or quantum size effect/zig-zag effect (intrinsic state emission), while the green emission is because of surface defects (defect state emission) [32]. The initial epoxy and carboxylic groups always induce non-radiative recombination of localized electron-hole pairs and hold back pristine emission. The surface modification leads to the fact that intrinsic state emission plays a major role in PL behaviors. On the other hand, carbonyl and epoxy were transformed into -OH groups in RGQDs, helping suppress non-radiative process and further improve integrity of π conjugated system as an electron donator (also reduced the

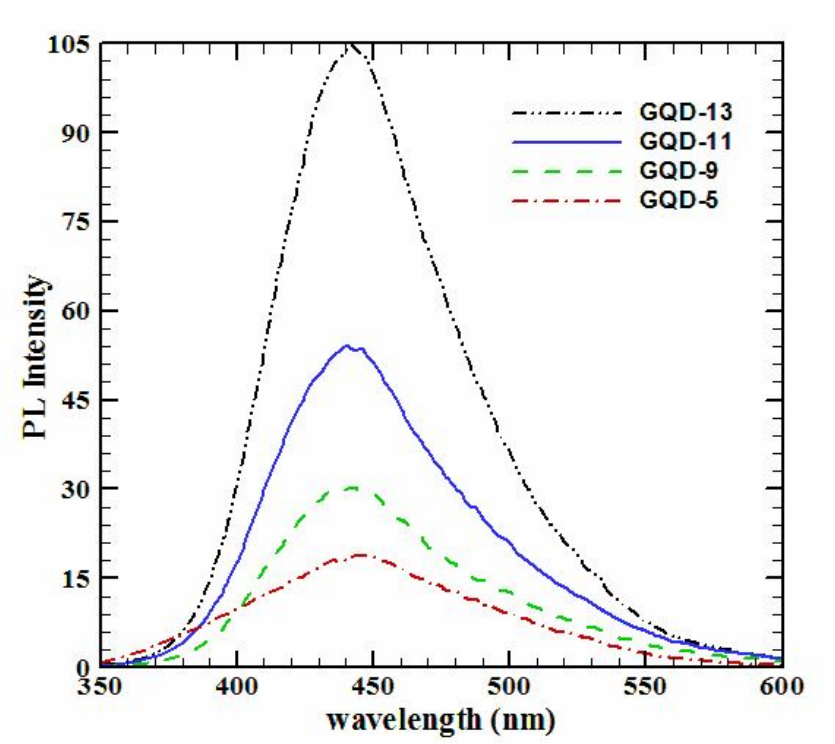

Fig. 10. Photoluminescence spectrum of GQDs.

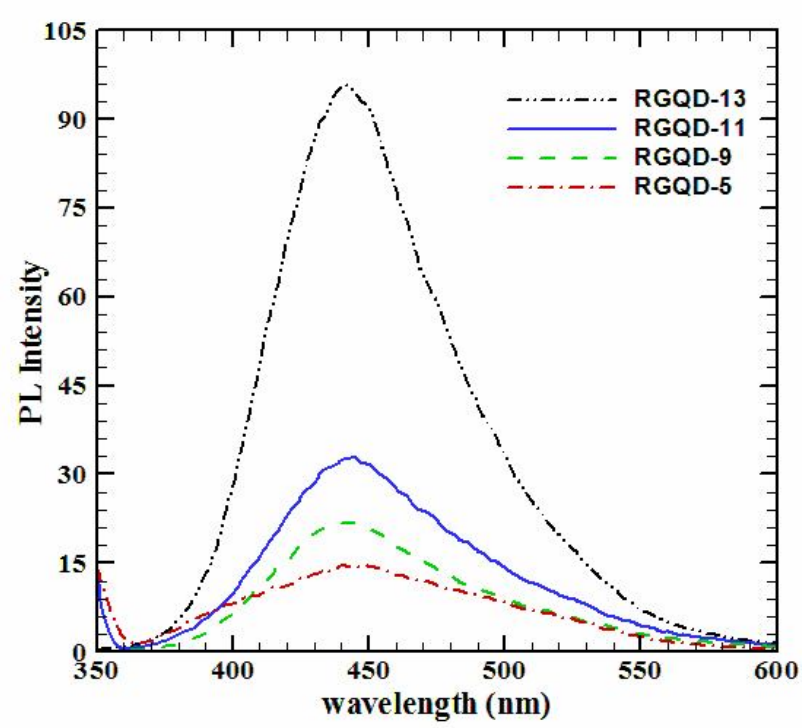

Fig. 11. Photoluminescence spectrum of RGQDs.

defects). Generally, both modification and reduction can adjust GQDs surface chemistry groups and alter the fluorescence color from green to blue. Also, reasonably RGQDs have larger bandgap than that of GQDs, because of suppression in non-radiative process as well as enriched electron density originated from -OH groups [32].

Some of research groups declared that the luminescence of GQDs was amplified by increasing sp^2 domains and electron-donating groups in GQDs through photochemical reduction and the hydrothermal procedure [33,34]. Comparison of Figs. 10 and 11 illustrates a fall in peak intensity after reduction of GQDs using laser irradiation which is probably due to surface modification and oxidation [35]. In a work performed by Rourke *et al*., they reported that the oxidation residual is responsible for the emission of GO [36].

Besides the change in PL wavelength, the overall PL was significantly intensified by increasing the pH. Pan et al. reported that PL of GQDs is intense at pH = 13, but significantly suppressed at pH = 5 [31,37]. Protonation and deprotonation of the functional groups are controlled by solvent pH, which will vary the charge and orientation of the functional groups and consequently GQDs' PL. At higher and lower pH, protonation and deprotonation increase degree of charge separation leading to a stronger dipole moment in the molecule. For pH > 10, emission starts from higher energy levels created by the complete ionization of -COOH and -OH groups [38].

At acidic pH, the electron donating nature of -COOH groups on the surface is more, because the possibility of the formation of -COO- is less. Accordingly, the -COOH group on the surface recedes the electrons from conduction band and hinder electron-hole recombination, so when the pH changes from 5 to 13, the fluorescence intensity enhances [39]. The carboxylic group on the surface becomes deprotonated (-COO-) by increasing the pH and the electron rejection efficiency reduces. Therefore, the electron-hole recombination is possible and the fluorescence enhances, which means the fluorescence quenching by decreasing pH from 13 to 5. Accordingly, when the pH increases from pH = 5 (acidic) to pH = 13 (basic), the ratio of -COOH to -COO- decreases. This is the reason for decreasing the intensity of fluorescence when pH = 13 is reduced to pH = 5, whereas the fluorescence intensity enhances by increasing pH [39]. Wang *et al*. have reported that the GQDs PL intensity changes in alkaline, neutral and acidic conditions, due to the aggregation of the GQDs [40]. Zhu *et al*. have figured out that the surface state/molecular state (molecular groups) are forcefully affected by the low and high pH [41]. In addition, the pH- dependence of PL behavior has been reported, indicating various PL mechanisms in different GQDs [31,32,37,42,43].

These results clearly demonstrated that the PL emission of GQDs can be tuned by the charge transfer between the functional groups and GQDs. The electron-withdrawing or electron-donating behavior of the functional groups can tune the bandgap of the GQDs and describe the PL peak shifts. Therefore, the charge distribution between the GQDs and the functional groups tunes and identifies the change of the bandgap in GQDs. This behavior concerns to the charge redistribution resulting from functionalization. Increasing the electron density can cause the reducing bandgap of GQDs which is similar to increasing the size of the GQDs [44].

Unfortunately, no single theory can easily define all the behaviors of GQDs. Usually GQDs are synthesized via various approaches, leading to diverse chemical structures of GQDs with different sizes and chemical compositions. Therefore, no reason with a deterministic feature can explain PL variations.

CONCLUSIONS

In summary, GQDs have been produced successfully by hydrothermal approach. FTIR proved fabrication of the GQDs. Pulse laser was implemented to adjust the bandgap and size of GQDs. The effect of important parameters such as pH on the bandgap and size of GQDs was investigated. It was observed that tuning the bandgap and size of GQDs could be achieved by changing the GQDs' pH. It was revealed that by raising the pH, agglomeration is improved leading to larger sizes. Absorption was enhanced via increasing pH. RGQDs showed higher absorption in comparison with GQDs. In order to study the change in bandgap, UV analysis was applied which was an evidence to the fact that the bandgap can be tuned. Increasing the bandgap was observed via calculating indirect bandgap of RGQDs. After laser irradiation, wider bandgap and hence

smaller GQDs size were obtained. Based on DLS, the size of GQDs is decreased after laser irradiation and increased by pH enhancement. SEM images displayed expansion in GQDs size due to pH growing and smaller size for RGQDs. The blue-shift in PL spectrum confirmed indirect bandgap calculation and declined in size of RGQDs.

The PL results were considerably affected by the nature of the functional groups on the surface. Due to the Protonation and deprotonation properties of functional groups, the electron transfer may take place to adjust the fluorescence intensity. The charge transfer between GQDs and functional groups can tune the GQDs bandgap, and consequently the PL emission due to the changing electron density in the GQDs.

This research suggests a simple, efficient and optimal method for the PL tuning of GQDs and a possible mechanism for changing the bandgap through functionalization.

This synthesis process of the GQDs and RGQDs leads to produce materials that will be beneficial for future graphene-based optoelectronic in a wide field of applications where size and band structures are important.

REFERENCES

[1] Wu, Y. M.; Zhang, X.; Jie, J. S.; Xie, C.; Zhang, X.; Sun, B. Q.; Wang, Y. Gao, P., Graphene transparent conductive electrodes for highly efficient silicon nanostructures-based hybrid heterojunction solar cells. *J. Phys. Chem. C.* **2013**, *117*, 11968-11976, DOI: 10.1021/jp402529c.

[2] Peng, J.; Gao, W.; Gupta, B. K.; Liu, Z.; Romero-Aburto, R.; Ge, L.; Song, L.; Alemany, L. B.; Zhan, X.; Gao, G.; Vithayathil, S. A.; Kaipparettu, B. A.; Marti, A. A.; Hayashi, T.; Zhu, J. J.; Ajayan, P. M., Graphene quantum dots derived from carbon fibers. *Nano Lett.* **2012**, *12*, 844-849, DOI: 10.1021/nl2038979.

[3] Liu, Q.; Guo, B.; Rao, Z.; Zhang, B.; Gong, J. R., Strong two-photon-induced fluorescence from photostable, biocompatible nitrogen-doped graphene quantum dots for cellular and deep tissue imaging. *Nano Lett.* **2013**, *13*, 2436-2441, DIO: 10.1021/nl400368v.

[4] Alivisatos, A. P., Semiconductor Clusters, Nanocrystals, and Quantum Dots. Science Vol. 1996, 271, Issue 5251, 933-937, DOI: 10.1126/science.271.5251.933.

[5] Kongkanand, A.; Tvrdy, K.; Takechi, K.; Kuno, M.; Kamat, P. V., Quantum dot solar cells tuning Pphotoresponse through size and shape control of CdSe-TiO_2 architecture. *J. Am. Chem. Soc.* **2008**, *130*, 4007-4015, DOI: 10.1021/ja0782706.

[6] Zhao, Q. D.; Xie, T. F.; Peng, L. L.; Lin, Y. H.; Wang, P.; Peng, L.; Wang, D. J., Size- and orientation-dependent photovoltaic properties of ZnO nanorods. *J. Phys. Chem. C* **2007**, *111*, 17136. 130, 4007, DOI: 10.1021/jp075368y.

[7] Long, R., Understanding the electronic structures of graphene quantum dot physisorption and chemisorption onto the TiO_2 (110) surface: A first-principles calculation. *Chem. Phys. Chem.,* **2013**, *14*, 579-582, DOI: 10.1002/cphc.201200882.

[8] Scholes, G. D.; Rumbles, G., Exciton in nanoscale systems. *Nat. Mater.* **2006**, *5*, 683-696, DOI: 10.1038/nmat1710.

[9] Brus, L. E., Carbon nanotubes, CdSe nanocrystals, and electron-electron interaction. *Nano Lett.* **2010**, *10*, 363-365, DOI: 10.1021/nl904263b.

[10] Fatimy, A. E.; Myers-Ward, R. L.; Boyd, A. K.; Daniels, K. M.; Gaskill, D. K.; Barbara, P., *Nature Nanotech*. **2016**, *11*, 335, DOI: 10.1038/nnano.2015.303.

[11] Muller, E. B.; Stouthamer, A. H.; Vanverseveld, H. W.; Eikelboom, D. H., Aerobic domestic waste water treatment in a pilot plant with complete sludge retention by cross-flow filtration. *Water. Res.* **1995**, *29*, 1179, DOI: 10.1016/0043-1354(94)00267-B.

[12] Daufin, G.; Escudier, J. P.; Carrere, H.; Berot, S.; Fillaudeau, L.; Decloux, M., Recent and emerging applications of membrane processes in the food and dairy industry. *Food Bioprod. Process.* **2001**, *79*, 89, DOI: 10.1016/S0960-3085(01)70244-1.

[13] Ruquan, Y., *et al*., Bandgap engineering of coal-derived graphene quantum dots, *ACS Appl. Mater. Interfaces* **2015**, *7*, 7041-7048, DOI: 10.1021/acsami.5b01419.

[14] Zibo, L., *et al*., Tuning the bandgap of graphene

quantum dots by gold nanoparticle-assisted O_2 plasma etching, *RSC Adv.,* **2016**, *6*, 97853-97860, DOI: 10.1039/c6ra16409a.

[15] Kumar, G. S.; Roy, R.; Sen, D.; Ghorai, U. K.; Thapa, R.; Mazumder, N.; Saha, S.; Chattopadhyay, K. K., Amino-functionalized graphene quantum dots: Origin of tunable heterogeneous photoluminescence. *Nanoscale.* **2014**, *6*, 3384-3391, DOI: 10.1039/ c3nr05376h.

[16] Willamson, A. J.; Franceschetti, A.; Fu, H.; Wang, L. W.; ZUNGER, A., Indirect band gaps in quantum dots made from direct-gap bulk materials. *J. Electronic Mater.*, **1999**, *28*, 5, DOI: 10.1007/s11664-999-0089-8.

[17] Kimiagar, S.; Rashidi, N.; Witkowski, B. S., Basic blue 41 removal by microwave hydrothermal reactor reduced graphene oxide. *Desalination and* Water *Treatment.* **2016**, *57*, 27269-27278, DOI: 10.1080/ 19443994.2016.1174743.

[18] Wang, L.; Wang, Y.; Xu, T.; Liao, H.; Yao, C.; Liu, Y.; Li, Z.; Chen, Z.; Pan, D.; Sun, L.; Wu, M., Gram-scale synthesis of single-crystalline graphene quantum dots with superior optical properties. *Nature Commun.* **2014**, *5*, 5357, DOI: 10.1038/ ncomms6357.

[19] Naebe, M.; Wang, J.; Amini, A.; Khayyam, H.; Hameed, N.; Li, L. H.; Chen, Y.; Fox, B., Mechanical property and structure of covalent functionalised graphene. *Nanocomposites* **2014**, *4*, 4375, DOI: 10.1038/srep04375.

[20] Pham, V. H.; Cuong, T. V.; Hur, S. H.; Oh, E.; Kim, E. J.; Shina, E. W.; Chung, J. S., Chemical functionalization of graphene sheets by solvothermal reduction of a graphene oxide suspension in N-methyl-2-pyrrolidone. *J. Mater. Chem.* **2011**, *21*, 3371-3377, DOI: 10.1039/c0jm02790a.

[21] Riesen, H.; Wiebeler, C.; Schumacher, S., Optical spectroscopy of graphene quantum dots. *J. Phys. Chem. A.* **2014**, *118*, DOI: 10.1021/jp502753a.

[22] Diao, S.; Zhang, X.; Shao, Z.; Ding, K.; Jie, J.; Zhang, X.; 12.35% Efficient graphene quantum dots/silicon heterojunction solar cells using graphene transparent electrode, *Nano Energy* **2017**, *31*, 359-366, DOI: 10.1016/j.nanoen.2016.11.051.

[23] Ritter, K. A.; Lyding, J. W., The influence of edge structure on the electronic properties of graphene quantum dots and nanoribbons. *Nat. Mater.* **2009**, *8*, 235-242, DOI: 10.1038/nmat2378.

[24] Lu, J.; Yeo, P. S. E.; Gan, C. K.; Wu, P.; Loh, K. P., Transforming C60 molecules into graphene quantum dots. *Nat. Nanotechnol.* **2011**, *6*, 247-252, DOI: 10.1038/ncomms3943.

[25] Murdock, R. C.; Braydich-Stolle, L.; Schrand, A. M.; Schlager, J. J.; Saber, H. M., Characterization of nanomaterial dispersion in solution prior to in vitro exposure using dynamic light scattering technique. *Toxicol. Sci.* **2008**, *101*, 239-253, DOI: 10.1093/ toxsci/kfm240.

[26] Jiang, J.; Oberdorster, G.; Biswas, P., Characterization of size, surface charge and agglomeration state of nanoparticle dispersions for toxicological studies. *J. Nanopart Res.* **2009**, *11*, 77-89, DOI: 10.1007/ s11051-008-9446-4.

[27] Bao, L.; Zhang, Z. L.; Tian, Z. Q.; Zhang, L.; Liu, C.; Lin, Y.; Qi, B.; Pang, D. W., Electrochemical tuning of luminescent carbon nanodots: from preparation to luminescence mechanism. *Adv. Mater.* **2011**, *23*, 5801, DOI: 10.1002/adma.201102866.

[28] Loh, K. P.; Bao, Q.; Eda, G.; Chhowalla, M., Graphene oxide as a chemically tunable platform for optical applications. *Nat. Chem.* **2010**, *2*, 1015, DOI: 10.1038/nchem.907.

[29] Zhu, S; Zhang, J.; Qiao, C.; Tang, S.; Li, Y.; Yuan, W.; Li, B.; Tian, L.; Liu, F.; Hu, R.; Gao, H.; Wei, H.; Zhang, H.; Sun, H.; Yang, B., Strongly green-photoluminescent graphene quantum dots for bioimaging applications. *Chem. Commun.* **2011**, *47*, 6858, DOI: 10.1039/c1cc11122a.

[30] Eda , G.; Lin , Y. Y.; Mattevi , C.; Yamaguchi , H.; Chen , H. A.; Chen , I. S.; Chen , C. W. ; Chhowalla , M. , Blue photoluminescence from chemically derived graphene oxide. *Adv. Mater.* **2010**, *22*, 505, 10.1002/ adma.200901996.

[31] Pan, D.; Zhang, J.; Li, Z.; Wu, M., Hydrothermal route for cutting graphene sheets into blue-luminescent graphene quantum dots. *Adv. Mater.* **2010**, *22*, 734, DOI: 10.1002/adma.200902825.

[32] Zhu, S.; Zhang, J.; Tang, A.; Qiao, C.; Wang, L.; Wang, H.; Liu, X.; Li, B.; Li, Y.; Yu, W.; Wang, X.;

Sun, H.; Yang, B., Surface chemistry routes to modulate the photoluminescence of graphene quantum dots: from fluorescence mechanism to up-conversion bioimaging applications. *Adv. Funct. Mater.* **2012**, *22*, 4732-4740, DOI: 10.1002/ adfm.201201499.

[33] Sun, H.; Wu, L.; Gao, N.; Ren, J.; Qu, X., Improvement of photoluminescence of graphene quantum dots with a biocompatible photochemical reduction pathway and its bioimaging application. *ACS Appl. Mater.* **2013**, *5* 1174-1179, DOI: 10.1021/am3030849.

[34] Sun, H.; Gao, N.; Wu, L.; Ren, J.; Wei, W.; Qu, X., Highly photoluminescent amino functionalized graphene quantum dots used for sensing copper ions. *Chem. Eur. J.* **2013**, *19* 13362-13368, DOI: 10.1002/ chem.201302268.

[35] Ghadim, E. E.; Rashidi, N.; Kimiagar, S.; Akhavan, O.; Manouchehrie, F.; Ghaderi, E., Pulsed laser irradiation for environment friendly reduction ofgraphene oxide suspensions, *Appl. Surf. Sci.* **2014**, *301*, 183-188. DOI: 10.1016/ j.apsusc.2014.02.

[36] Thomas, H. R.; Valles, C.; Young, R. J.; Kinloch, I. A.; Wilson, N. R.; Rourke, J. P., Identifying the fluorescence of graphene oxide, *J. Mater. Chem. C* **2013**, *1*, 338-342. DOI: 10.1039/C2TC00234E.

[37] Huang, H.; Li, J.; Zhang, Z.; Yu, W.; Chen, Z.; Li, Z., Cutting sp2clusters in graphene sheets into colloidal graphene quantum dots with strong green fluorescence, *J. Mater. Chem.* **2012**, *22*, 3314-3318, DOI: 10.1039/C2JM16005F.

[38] Syamantak, K.; Abhishek, G.; Navneet, C. V.; Chayan, K. N., Time-resolved emission reveals ensemble of emissive states as the origin of multicolor fluorescence in carbon dots, *Nano Lett.* **2015**, *15*, 8300, DOI: 10.1021/ acs.nanolett.5b03915.

[39] Namasivayam, D.; King-Chuen L., Raghupathy suresh, and perumal ramamurthy, unravelling the multiple emissive states in citric acid-derived Carbon-dots, *J. Phys. Chem. C* **2016**, *120*, 1252, DOI: 10.1021/acs.jpcc.5b08516.

[40] Liang, W.; Weitao, L.; Bin, W.; Zhen, L.; Dengyu, P.; Minghong, W., Room-temperature synthesis of graphene quantum Dots *via* electron-beam irradiation and their application in cell imaging, *Chem. Engin. J.,* **2016**, *300*, 75-82, DOI:10.1016/j.cej.2016.10.022.

[41] Zhu, S.; Meng, Q.; Wang, L.; Zhang, J.; Song, Y.; Jin, H.; Zhang, K.; Sun, H.; Wang, H.; Yang, B., Highly photoluminescent carbon dots for multicolor patterning, sensors and bioimaging. *Angew. Chem. Int. Ed.* **2013**, *52*, 3953-3957, DOI: 10.1002/ anie.201300519.

[42] Wenkai, Z., *et al.*, Graphenol defects induced blue emission enhancement in chemically reduced graphene quantum dots Phys. *Chem. Chem. Phys.* **2015**, *17*, 22361, DOI: 10.1039/x0xx00000x.

[43] Zhu, S. J.; J. Zhang, H.; Liu, X.; Li, B.; Wang, X. F.; Tang, S. J.; Meng, Q. N.; Li, Y. F.; Shi, C.; Hu, R.; Yang, B., Graphene quantum dots with controllable surface oxidation, tunable fluorescence and up-conversion emission, *RSC Adv.,* **2012**, *2*, 2717, DOI: 10.1039/C2RA20182H.

[44] Osaka, T.; Mccullough, R. D., Advances in molecular design and synthesis of regioregular polythiophenes. *Acc. Chem. Res.* **2008**, *41*, 1202-1214, DOI: 10.1021/ ar800130s.